Supporting Information

Ohgami et al. 10.1073/pnas.1004520107

SI Materials and Methods

After perfusion fixation by Bouin's solution, cochleae from 0.5- to 18-d-old and 1- to 14-mo-old mice were immersed in the same solution overnight and for 1 wk, respectively. Immunohistochemical analysis with anticleaved caspase-3 (1:500; Epitomics, Inc.) was performed with paraffin sections. The VECTASTAIN ABC kit (Vector) and Envision kit/HRP (diaminobenzidine; DAKO) were used in both of the immunohistochemical analyses with counterstained hematoxylin. TUNEL with 4% (vol/vol) paraformaldehyde fixative solution was performed following the instructions of the manufacturer (Chemicon), with a previously reported positive control of hair bulge cells (1). To estimate the number of intermediate cells between c-Ret-KI$^{Y1062F/Y1062F}$ mice and littermate WT mice morphologically, c-Ret-KI$^{Y1062F/Y1062F}$;Dct-LacZ-Tg mice were newly established by crossing c-Ret-KI$^{Y1062F/+}$ mice with Dct-LacZ-Tg mice (2). After fixation with PBS containing 0.25% glutaraldehyde, the inner ears were stained with X-gal, as previously reported (3).

1. Ito M, Kizawa K, Toyoda M, Morohashi M (2002) Label-retaining cells in the bulge region are directed to cell death after plucking, followed by healing from the surviving hair germ. *J Invest Dermatol* 119:1310–1316.
2. Mackenzie MA, Jordan SA, Budd PS, Jackson IJ (1997) Activation of the receptor tyrosine kinase kit is required for the proliferation of melanoblasts in the mouse embryo. *Dev Biol* 192:99–107.
3. Yajima I, Larue L (2008) The location of heart melanocytes is specified and the level of pigmentation in the heart may correlate with coat color. *Pigment Cell Melanoma Res* 21:471–476.

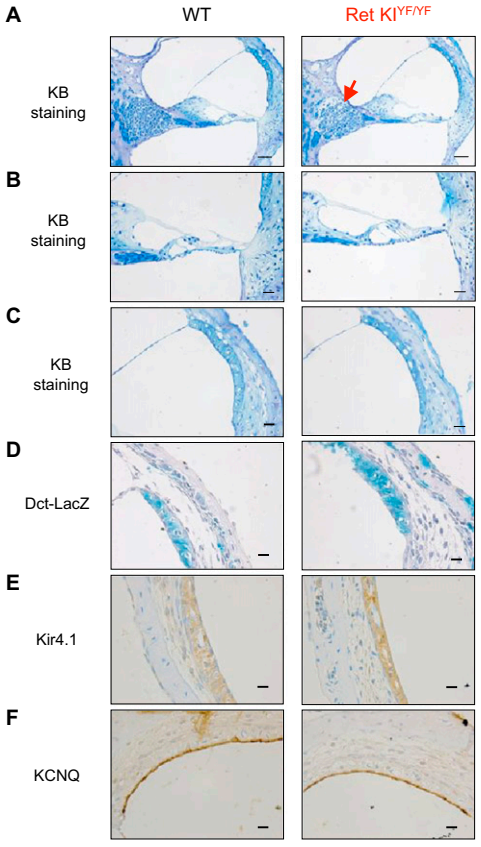

Fig. S1. Morphological analyses of inner ears from c-Ret-KI$^{Y1062F/Y1062F}$ mice and littermate WT mice. (*A–C*) Light microscopy showed no morphological differences of inner ears (*A*), the organ of Corti (*B*), or the stria vascularis (*C*) with Kluver–Barrera (KB) staining between 12-d-old c-Ret-KI$^{Y1062F/Y1062F}$ mice (Ret KI$^{YF/YF}$, *Right*) and littermate WT mice (WT, *Left*), except for SGNs (red arrow in *A*). (*D–F*) Light microscopy showed no significant differences of the stria vascularis between 14-d-old c-Ret-KI$^{Y1062F/Y1062F}$ mice (*Right*) and littermate WT mice (WT, *Left*). (*D*) LacZ staining of Dct-LacZ^{+} intermediate cells. (*E*) Immunohistochemical analysis of the stria vascularis with anti-Kir4.1 antibody (1:500; Santa Cruz), known as one of the intermediate cell markers in the stria vascularis (1). (*F*) Immunohistochemical analysis of the stria vascularis with anti-KCNQ (1:50; Santa Cruz), known as one of the marginal cell markers in the stria vascularis (1). (Scale bars: *A*, 50 μm; *B–F*, 20 μm.)

1. Knipper M, et al. (2006) Deafness in LIMP2-deficient mice due to early loss of the potassium channel KCNQ1/KCNE1 in marginal cells of the stria vascularis. *J Physiol* 576:73–86.

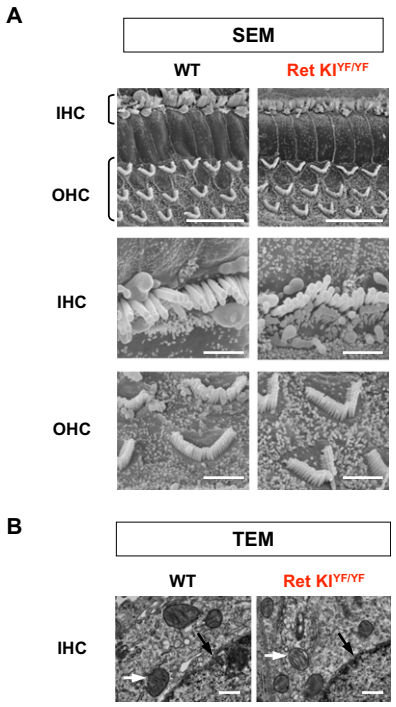

Fig. S2. Morphological analyses of hair cells from 18-d-old c-Ret-KI$^{Y1062F/Y1062F}$ mice and littermate WT mice. (*A*) SEM showed no morphological differences of inner hair cells (IHC) and outer hair cells (OHC) at equivalent positions between c-Ret-KI$^{Y1062F/Y1062F}$ mice (Ret KI$^{YF/YF}$, *Right*) and littermate WT mice (WT, *Left*). Glutaraldehyde (2%; vol/vol)- and paraformaldehyde (2%; vol/vol)-fixed inner ears were microdissected, stepwise dehydrated in ethanol solutions, and eventually dried up to a critical point. Prepared inner ears were then mounted on aluminum stubs with colloidal silver adhesive and sputter-coated with gold palladium before imaging using a Hitachi S-800s scanning electron microscope. (*B*) TEM for IHCs at equivalent positions between c-Ret-KI$^{Y1062F/Y1062F}$ mice (Ret KI$^{YF/YF}$, *Right*) and littermate WT mice (WT, *Left*). Nucleus (black arrows) and mitochondria (white arrows) showed comparable morphology in WT and c-Ret-KI$^{Y1062F/Y1062F}$ mice. (Scale bars: *A Top*, 15 μm; *A Middle* and *Bottom*, 3 μm; *B*, 500 nm.)

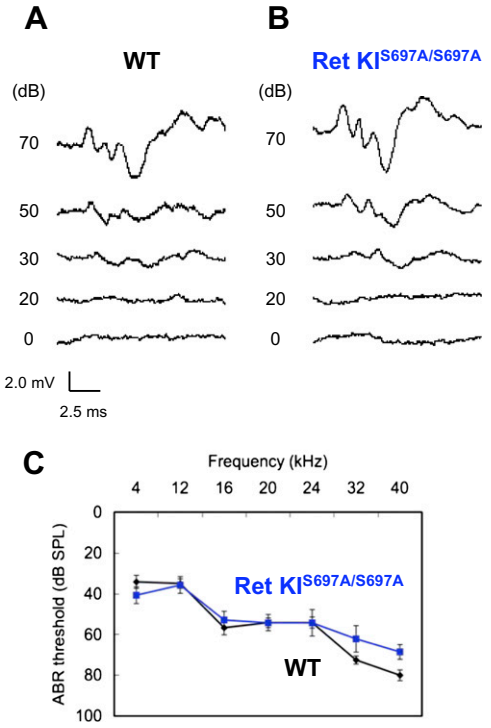

Fig. S3. Hearing levels of 18-d-old homozygous c-Ret S697A KI mice (c-Ret-KI$^{S697A/S697A}$ mice) and littermate WT mice. ABR waveforms of 18-d-old littermate WT mice (*A*) and c-Ret-KI$^{S697A/S697A}$ mice (1) (*B*) at 0- to 70-dB SPL at 12 kHz are presented. (*C*) Comparable hearing levels (mean ± SE) in 18-d-old c-Ret-KI$^{S697A/S697A}$ mice (Ret KI$^{S697A/S697A}$, blue squares, $n = 8$) and littermate WT mice (WT, black squares, $n = 8$) are presented.

1. Asai N, et al. (2006) Targeted mutation of serine 697 in the Ret tyrosine kinase causes migration defect of enteric neural crest cells. *Development* 133:4507–4516.

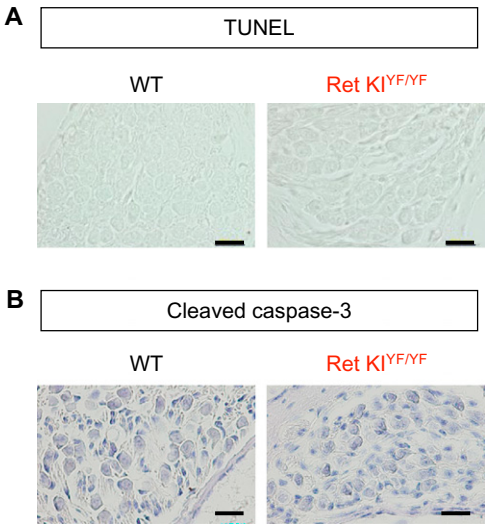

Fig. S4. No apoptotic signals were detected in SGNs from homozygous c-Ret Y1062F KI mice (c-Ret-KI$^{Y1062F/Y1062F}$ mice) and littermate WT mice. (*A*) SGNs from 14-d-old c-Ret-KI$^{Y1062F/Y1062F}$ mice (Ret KI$^{YF/YF}$) and littermate WT mice stained by the TUNEL method were observed under a differential interference contrast microscope. (*B*) Results of immunohistochemical analysis for serial sections of the levels of cleaved caspase-3 expression at SGNs from 14-d-old WT mice and c-Ret-KI$^{Y1062F/Y1062F}$ mice (Ret KI$^{YF/YF}$). These specimens were developed with diaminobenzidine, followed by counterstaining with hematoxylin. (Scale bars: 20 μm.) Representative results of four independent experiments with consistent results are shown in *A* and *B*.

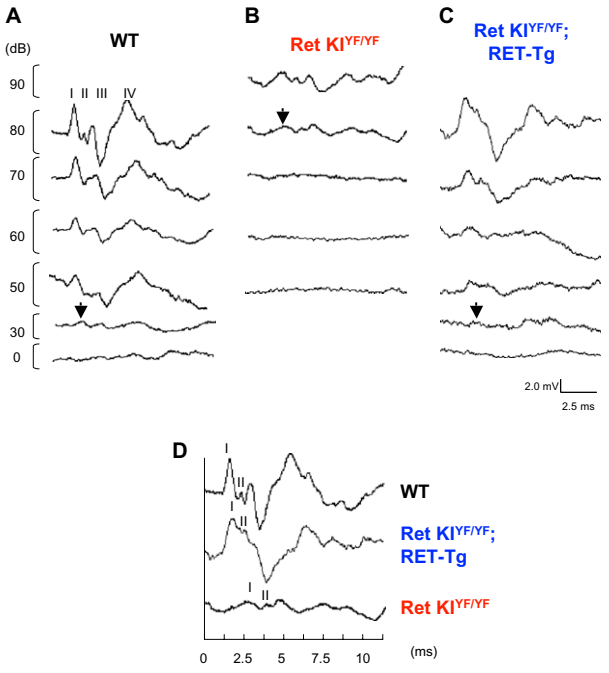

Fig. S5. Representative ABR recordings from WT mice, homozygous c-Ret Y1062F KI mice (c-Ret-KI$^{Y1062F/Y1062F}$ mice), c-Ret-KI$^{Y1062F/Y1062F}$ mice with constitutively activated RET (c-Ret-KI$^{Y1062F/Y1062F}$;RET-Tg mice) and constitutively activated RET-Tg mice. ABR waveforms of 21-mo-old WT mice (WT, *A*), littermate c-Ret-KI$^{Y1062F/Y1062F}$ mice (Ret KI$^{YF/YF}$, *B*), and c-Ret-KI$^{Y1062F/Y1062F}$;RET-Tg mice (Ret KI$^{YF/YF}$;RET-Tg, *C*) at 0- to 90-dB SPL at 12 kHz are presented. (*A*) Peaks of ABR waves I, II, III, and IV are indicated in WT mice. WT mice (*A*) and c-Ret-KI$^{Y1062F/Y1062F}$;RET-Tg mice (*C*) showed comparable ABR wave peaks, whereas no ABR wave peaks up to 70-dB SPL were observed in c-Ret-KI$^{Y1062F/Y1062F}$ mice (*B*). Arrows indicate wave I peaks corresponding to ABR threshold levels. (*D*) Comparable interpeak latencies for waves I–II (auditory nerve) at 80-dB SPL were shown in WT (0.8 ms) and c-Ret-KI$^{Y1062F/Y1062F}$;RET-Tg mice (Ret KI$^{YF/YF}$;RET-Tg; 0.83 ms), whereas c-Ret-KI$^{Y1062F/Y1062F}$ mice showed delayed interpeak latency for waves I–II (1.25 ms). The peaks of ABR waves I and II are indicated in each mouse line.

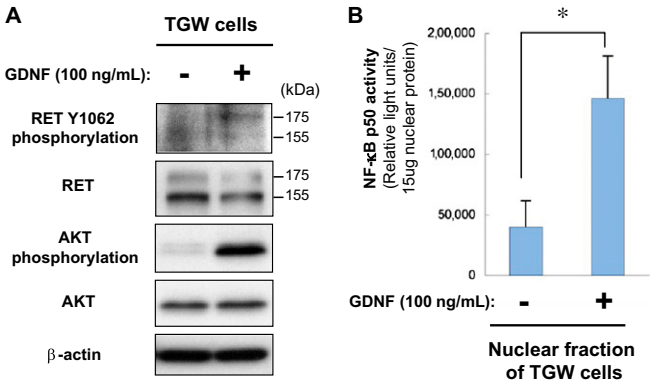

Fig. S6. Ret Y1062-mediated signaling pathway modulates NF-κB p50 activity via Akt in neural cells. The human neuroblastoma cell line TGW was incubated in the absence (–) or presence (+) of 100 ng/mL GDNF for 15 min at 37 °C, as previously reported (1, 2). (*A*) GDNF-mediated phosphorylation levels of Y1062 in c-RET and AKT in TGW cells. Western blotting of the cell lysates with anti-RET Y1062 phosphorylation (1:200; Santa Cruz), anti-c-RET (1:300; Immuno Biological Laboratories), anti-Akt phosphorylation (1:1,000; Cell Signaling), anti-Akt (1:1,000; Cell Signaling), and anti-β-actin (1:5,000; Sigma) antibodies. (*B*) Levels of NF-κB p50 activity. After incubation of TGW cells in the absence (–) or presence (+) of 100 ng/mL GDNF for 15 min at 37 °C, the nuclear fractions were extracted from the neural cells by using an NE-PER Nuclear Extract and Cytoplasmic Extraction Reagents kit according to the instructions of the manufacturer (PIERCE). After nuclear extraction, NF-κB p50 activity was detected using an EZ-Detect transcription factor kit (PIERCE), as previously reported (3, 4). Briefly, active NF-κB p50 in the nuclear fraction binds to the consensus sequence immobilized to a 96-well plate and is then incubated with anti-p50 antibody, followed by detection of a chemiluminescent signal. Significant difference (*$P < 0.01$) from the control was analyzed by the Mann–Whitney *U* test.

1. Jijiwa M, et al. (2004) A targeting mutation of tyrosine 1062 in Ret causes a marked decrease of enteric neurons and renal hypoplasia. *Mol Cell Biol* 24:8026–8036.
2. Hayashi H, et al. (2000) Characterization of intracellular signals via tyrosine 1062 in RET activated by glial cell line-derived neurotrophic factor. *Oncogene* 19:4469–4475.
3. Choi DS, Young H, McMahon T, Wang D, Messing RO (2003) The mouse RACK1 gene is regulated by nuclear factor-kappa B and contributes to cell survival. *Mol Pharmacol* 64: 1541–1548.
4. Lee S, Rivier C (2005) Role played by hypothalamic nuclear factor-kB in alcohol-mediated activation of the rat hypothalamic-pituitary-adrenal axis. *Endocrinology* 146:2006–2014.

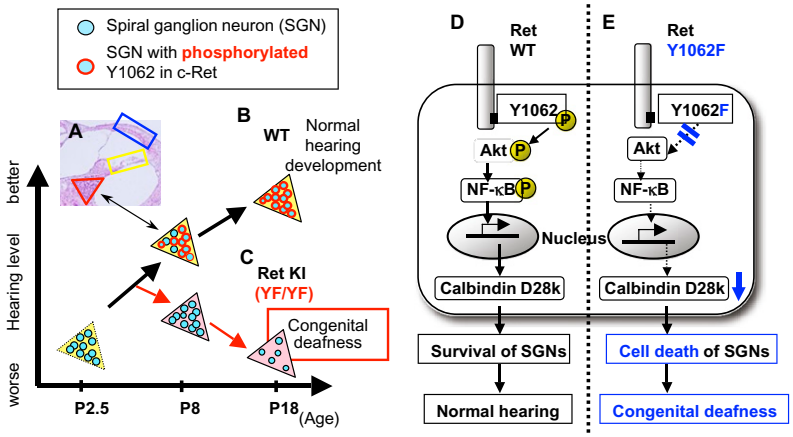

Fig. S7. Schematic summary of the major findings obtained in this study. (*A*) Inner ear from a WT mouse at P14 stained with H&E. Red triangle, yellow square, and blue square contain SGNs, inner and outer hair cells, and the stria vascularis, respectively. Our morphological analyses showed almost no abnormalities in these areas other than SGNs from c-Ret-KI$^{Y1062F/Y1062F}$-mice (Figs. S1 and S2). (*B* and *C*) Colored triangles in the schema represent Rosenthal's canals in WT mice (yellow triangles) and homozygous c-Ret-KI$^{Y1062F/Y1062F}$ mice [Ret KI (YF/YF), pink triangles] (1). Blue circles with a black line in the triangles represent SGNs. Blue circles with a red line in the triangles represent SGNs with "phosphorylated Y1062 in c-Ret." The *x* axis and *y* axis indicate the age of the mice and hearing levels, respectively. (*B*) WT mice showed that c-Ret protein was constantly expressed in SGNs (P1–18), whereas the numbers of Y1062-phosphorylated SGNs (blue circles with red line in yellow triangles) were sharply increased around P6–7, several days before the WT mice begin to acquire intact hearing levels (around P12) (Fig. 1). (*C*) c-Ret-KI$^{Y1062F/Y1062F}$ mice suffered from congenital deafness with decreased cell density of SGNs. c-Ret-KI$^{Y1062F/Y1062F}$ mice showed no Y1062-phosphorylated SGNs even on P14 (Figs. 2 and 3), although the number of Y1062-phosphorylated SGNs began to increase in WT mice from P6 (Fig. 1). Congenital hearing loss in c-Ret-KI$^{Y1062F/Y1062F}$ mice was rescued by introducing constitutively activated RET (Fig. 4). (*D* and *E*) Schematic illustration of a mechanistic model for c-Ret–mediated congenital deafness with neuroedgeneration of SGNs in c-Ret-KI$^{Y1062F/Y1062F}$ mice. (*D*) WT mice acquire normal hearing with phosphorylation of the c-Ret Y1062-mediated signaling pathway. P, phosphorylation. (*E*) Impairments of the c-Ret Y1062-mediated signaling pathway (blue double line and downward dashed arrows) cause decreased expression of calbindin D28k (blue arrow) via Akt/NF-κB signaling, resulting in auditory nerve degeneration in c-Ret-KI$^{Y1062F/Y1062F}$ mice (c-Ret Y1062F). This figure was drawn on the basis of results of previous studies (2, 3) and results obtained in this study.

1. Jijiwa M, et al. (2004) A targeting mutation of tyrosine 1062 in Ret causes a marked decrease of enteric neurons and renal hypoplasia. *Mol Cell Biol* 24:8026–8036.
2. Hayashi H, et al. (2000) Characterization of intracellular signals via tyrosine 1062 in RET activated by glial cell line-derived neurotrophic factor. *Oncogene* 19:4469–4475.
3. Mattson MP, Camandola S (2001) NF-kappaB in neuronal plasticity and neurodegenerative disorders. *J Clin Invest* 107:247–254.

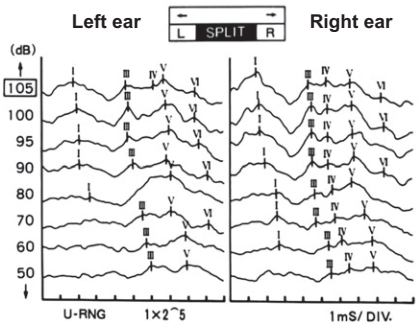

Fig. S8. Representative ABR recordings from an aganglionosis patient. ABR waveforms (thresholds of 50- to 70-dB SPL) of a representative deaf patient with a homozygous missense mutation at arginine 969 in c-RET are shown (listed as case no. 1 in Table S1). Healthy volunteers of similar ages showed ABR thresholds of 20-dB SPL. Seven ABR peaks correspond to cochlear nerve activity (wave I) and downstream neural activities (waves II–VII) (1, 2).

1. Møller AR, Jannetta PJ (1985) Neural generators of the auditory brainstem response. *The Auditory Brainstem Response*, ed Jacobson JT (Taylor & Francis, London), pp 13–31.
2. Stockard JJ, Rossiter VS (1977) Clinical and pathologic correlates of brain stem auditory response abnormalities. *Neurology* 27:316–325.

Table S1. RET-mediated intestinal aganglionosis patients with hearing loss

Case No.	Gender	Familial (F) or sporadic (S)	Range of aganglionosis	Hearing loss		Exon	Codon	Nucleotide change	Homozygous or heterozygous	Effect on coding sequence
				Right	Left					
1	M	S	Stomach to anorectum	+	+	17	969	CGG → TGG	Homozygous	Missense
2	F	S	Stomach to anorectum	–	–	10	588	GGC → GAC	Heterozygous	Missense
3	M	F	Duodenum to anorectum	+	+	1	13	37 deletion C	Heterozygous	Frameshift and stop at codon 22
4	M	S	Lig. of Treitz to anorectum	+	+	17	969	CGG → TGG	Heterozygous	Missense
5	F	S	Lig. of Treitz to anorectum	–	–	3	144	432 deletion C	Heterozygous	Frameshift and stop at codon 244
6	M	S	Jejunum to anorectum	–	–	15	897	CGA → CAA	Heterozygous	Missense
7	F	S	Jejunum to anorectum	–	–	2	30	TAC → TGC	Heterozygous	Missense
8	F	F	Ileum to anorectum	–	–	1	13	37 deletion C	Heterozygous	Frameshift and stop at codon 22
9	F	F	Ileum to anorectum	–	–	1	13	37 deletion C	Heterozygous	Frameshift and stop at codon 22
10	F	S	Ileum (distal) to anorectum	–	–	17	942	TGG → TGC	Heterozygous	Missense
11	M	S	Ileum (distal) to anorectum	–	–	12	734	GAA → AAA	Heterozygous	Missense
12	F	S	Ileum (distal) to anorectum	–	–	7	489	GAC → AAC	Heterozygous	Missense

Three patients with bilateral auditory system abnormalities were found in 12 patients who had intestinal aganglionosis with a c-*RET* mutation but no *GDNF*, *NTN*, *SOX10*, *EDNRB*, and *ET-3* mutations. All the patients with deafness, who had been previously reported to have congenital hearing losses without detection of their causal genes (1), were boys with total intestinal aganglionosis. F, female; Lig, Ligamentum; M, male.

1. Shimotake T, Iwai N (1994) Auditory brainstem response in children with total intestinal aganglionosis. *Lancet* 343:1362.